Nonlinear Control of a Shape Memory Alloy Actuated Manipulator

Mohammad H. Elahinia
Graduate Research Assistant

Hashem Ashrafiuon
Associate Professor,
Assoc. Mem. ASME
e-mail: hashem.ashrafiuon@villanova.edu

Mechanical Engineering Department,
Villanova University,
Villanova, PA 19085

This paper presents a nonlinear, robust control algorithm for accurate positioning of a single degree of freedom rotary manipulator actuated by Shape Memory Alloy (SMA). A model for an SMA actuated manipulator is presented. The model includes nonlinear dynamics of the manipulator, a constitutive model of Shape Memory Alloy, and electrical and heat transfer behavior of SMA wire. This model is used for open and closed loop motion simulations of the manipulator. Experiments are presented that show results similar to both closed and open loop simulation results. Due to modeling uncertainty and nonlinear behavior of the system, classic control methods such as Proportional-Integral-Derivative control are not able to present fast and accurate performance. Hence a nonlinear, robust control algorithm is presented based on Variable Structure Control. This algorithm is a control gain switching technique based on the weighted average of position and velocity feedbacks. This method has been designed through simulation and tested experimentally. Results show fast, accurate, and robust performance of the control system. Computer simulation and experimental results for different stabilization and tracking situations are also presented. [DOI: 10.1115/1.1501285]

1 Introduction

Shape Memory Alloys (SMAs) consist of a group of metallic materials that demonstrate the ability to return to some previously defined shape or size when subjected to the appropriate thermal procedure. The shape memory effect occurs due to a temperature and stress dependent shift in the materials crystalline structure between two different phases called Martensite and Austenite. Martensite, the low temperature phase, is relatively soft whereas Austenite, the high temperature phase, is relatively hard. The change that occurs within SMAs crystalline structure is not a thermodynamically reversible process and results in temperature hysteresis.

SMAs have been used in a variety of actuation, energy absorbing, and sensing applications. The key feature of this material is its ability to undergo large seemingly plastic strains and subsequently recover these strains when a load is removed or the material is heated. SMA actuators have several advantages for miniaturization such as excellent power to mass ratio, maintainability, reliability, and clean and silent actuation. The disadvantages are low energy efficiency due to conversion of heat to mechanical energy and inaccurate motion control due to hysteresis, nonlinearities, parameter uncertainties, and difficulty in measuring variables such as temperature.

Many of the SMA actuators depend on the mechanical amplification of the displacement either through the use of long straight fibers [1–7] or through the use of SMA coils [4,8–15]. There are two classes of SMA actuators. The one-way actuators (*bias type*) are composed of an SMA element and a bias spring [16]. The two-way actuators (*differential type*) are made of two SMA elements [2–4,9]. The differential type actuators have the advantage of easier and faster control while the bias type actuators require less power, making them more desirable for internally powered devices. The bias type actuators can be very slow if there is an overshoot thus requiring cooling and the work of the bias spring for reverse actuation.

Considerable research for modelling the microscopic and macroscopic behavior of SMAs has been performed in the past forty years. Since the mechanical behavior of SMAs is closely related to microscopic phase transformation, stress-strain based constitutive relations are not applicable to describe SMA behavior. There are two classes of shape memory alloy models: microscopic [17] and macroscopic [4,18–24]. We have used an improved macroscopic constitutive model based on the work presented by Liang [25] in combination with a heat convection model [26].

The control research applied to SMAs may be divided into three categories of linear control, Pulse Width Modulation (PWM), and nonlinear control. Different variations of linear Proportional Integral Derivative (PID) controls have been explored by several researchers [5,8,11,18,27,28] while many others have used PWM [3,4,9,16]. Several nonlinear control schemes have also been explored. Nakazato et al. [29] designed a fuzzy logic controller to control the duty cycle of a PWM controller. Kumagi et al. [30] used a neuro-fuzzy logic model in conjunction with a PD controller. Dickinson and Wen [31] applied a P-controller for stabilizing an SMA actuator pulse and an adaptation scheme to compensate for steady state error. Arai et al. [32] used feedback linearization for SMA. Choi and Choeung [33] have applied variable structure control (VSC) to manage the vibration of a flexible beam. VSC [34] has also been used by Grant and Hayward for position control [35], vibration isolation [36], and force control [37] of the differential type actuators using a linear model.

In this work, we have developed a nonlinear control algorithm based on VSC for accurate and quick positioning of a single-degree-of-freedom (1dof) rotary arm. The arm is actuated by a bias type actuator constructed with SMA wire, pulleys, and a linear spring. A nonlinear model is developed based on a nonlinear arm dynamic model, an SMA wire constitutive model, a nonlinear phase transformation model, and a nonlinear heat convection model. The VSC algorithm utilizes a switching control law to drive the nonlinear plant's state trajectory onto a user-specified surface in the state space, and to maintain it on this surface for all subsequent times. When the state trajectory of the plant is above the surface the control path has a given structure and when the trajectory drops below the surface, a different structure is applied. The controller is robust in spite of parameter uncertainties and nonlinearity in the model and external disturbances. The control algorithm is fast and efficient since it avoids actuator overshoot

Contributed by the Technical Committee on Vibration and Sound for publication in the JOURNAL OF VIBRATION AND ACOUSTICS. Manuscript received October 2001; Revised May 2002. Associate Editor: R. Ohayon.

and chattering. Several simulation and experimental results are presented to verify the effectiveness of the control algorithm.

2 The SMA Arm Model

The single degree-of-freedom (1-dof) SMA-actuated arm is shown in Fig. 1. The arm orientation is initially at −45 deg relative to the horizontal axis. We have used 150μm diameter Ni-Ti SMA wire which is actuated by electrical heating. The net actuating torque is the difference between the resulting bias spring and SMA wire torques. The dSpace™ *hardware in the loop* solution is used as a desktop controller board for experimental verification of simulations performed in the MATLAB™/Simulink environment.

An accurate model of the SMA actuated 1-dof arm is required for simulation and evaluation of different control algorithms. The model consists of phase transformation, heat transfer, SMA wire constitutive, and arm dynamic model blocks. In addition, there is an amplifier, an encoder, and a signal conditioner, as shown in Fig. 2. Elements of the models are bilaterally connected forming an algebraic loop.

2.1 Kinematic/Dynamic Model. The nonlinear dynamic model of the arm including spring and payload effects is:

$$I_e\ddot{\theta}=\tau_w(\sigma)-\tau_g(\theta)-\tau_s(\theta)-c\dot{\theta} \tag{1}$$

where τ_w, τ_g, and τ_s are the resulting torques from SMA wire, gravitational loads, and the bias spring, respectively, and σ is the wire stress. I_e is the effective mass moment of inertia of the arm, griper, and the payload, and c is the torsional damping coefficient which is needed to approximate the net joint friction.

The SMA wire strain rate $\dot{\varepsilon}$ and joint angular velocity $\dot{\theta}$ are related kinematically as

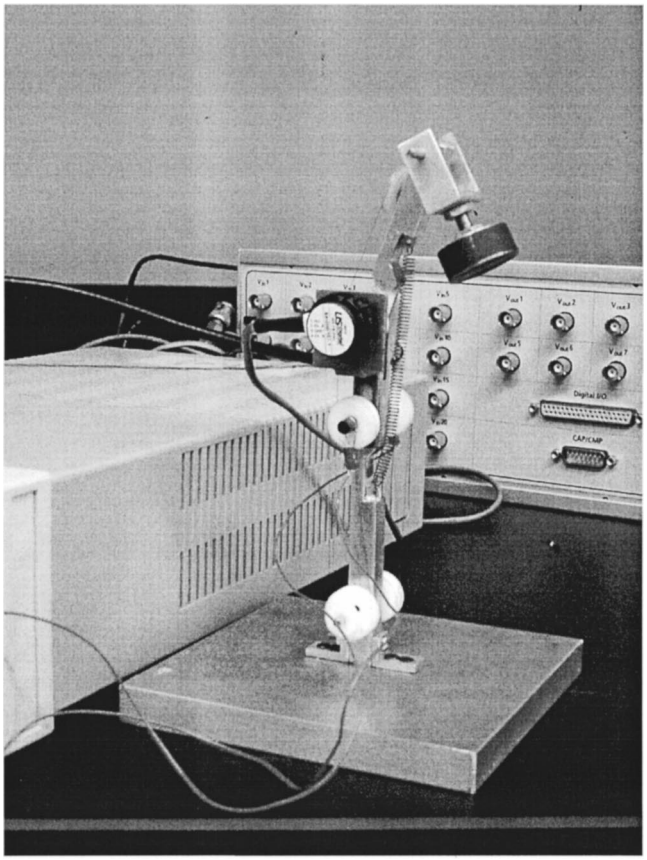

Fig. 1 The 1-dof SMA arm, actuated by NiTi wire and a bias spring

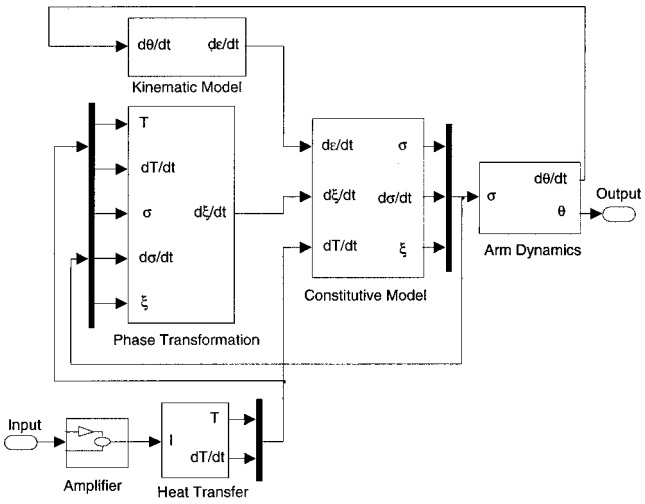

Fig. 2 Block diagram of the 1-dof SMA-actuated arm model

$$\dot{\varepsilon}=-\frac{2r\dot{\theta}}{l_0} \tag{2}$$

where r is the pulley radius and l_0 is the initial length of SMA wire.

2.2 Wire Constitutive Model. The wire constitutive model shows the relationship between stress rate ($\dot{\sigma}$), strain rate, and temperature rate ($\dot{T}$) [23]:

$$\dot{\sigma}=D\dot{\varepsilon}+\theta_T\dot{T}+\Omega\dot{\xi} \tag{3}$$

where $D=D_M+D_A/2$ is (the average) Young modulus, D_A is Austenite Young modulus, D_M is Martensite Young modulus, θ_T is thermal expansion factor, $\Omega=-D\varepsilon_0$ is phase transformation contribution factor, and ε_0 is the initial (i.e., maximum) strain [25].

Table 1 Modeling parameters and their numerical value (SI units)

Parameter	Description	Value
m	SMA wire's mass per unit length	$1.14e^{-4}$
A	SMA wire's cross-sectional area	$4.712e^{-4}$
l_0	Initial length of SMA wire	0.9
ε_0	SMA wire's initial strain	0.04
σ_0	SMA wire's initial stress	$75e^6$
ξ_0	SMA wire's initial Martensite faction factor	1
D_A	Austenite Young modulus	$75e^9$
D_M	Martensite Young modulus	$28e^9$
A_s'	Austenite start temperature	68
A_f'	Austenite final temperature	78
M_s'	Martensite start temperature	52
M_f'	Martensite final temperature	42
C_A	Austenite curve fitting parameter	$10.3e^6$
C_M	Martensite curve fitting parameter	$10.3e^6$
θ_T	SMA wire's thermal expansion factor	−0.055
c_p	Specific heat of SMA wire	200*4.187
R	SMA wire's resistance per unit length	50.8
T_∞	Ambient temperature	20
h_0	Heat convection constant coefficient	120
h_2	Heat convection second order coefficient	0.001
r	Pulley radius	$8.25e^{-3}$
m_p	Payload mass	0.0572
m_a	Arm mass	0.0187
k	Bias spring stiffness	3.871
l_{k0}	Bias spring initial length	0.03015

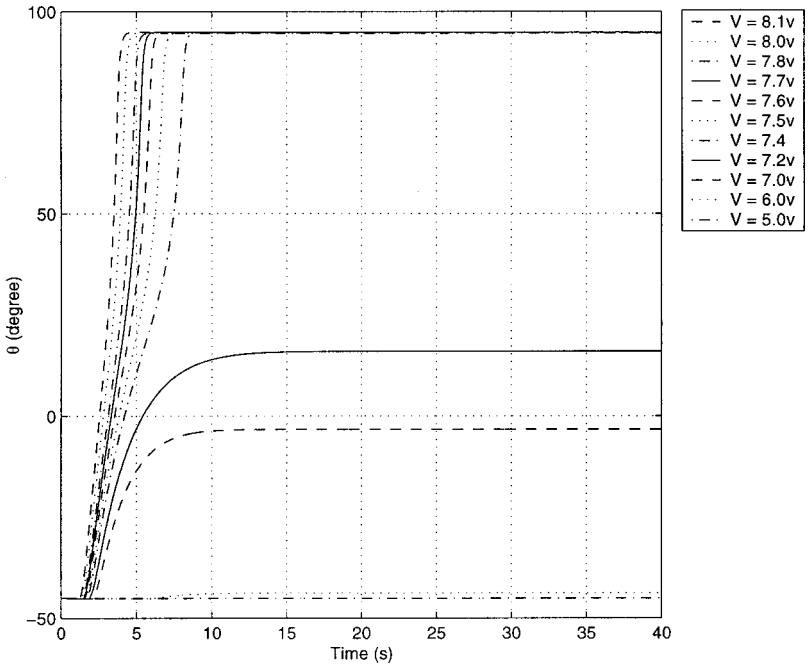

Fig. 3 Open loop simulation results in response to different step inputs

2.3 SMA Wire Phase Transformation Model. Due to hysteretic behavior of SMA wire, the phase transformation equations are different for heating and cooling. Heating results in reverse transformation from Martensite to Austenite:

$$\xi = \frac{\xi_M}{2}\{\cos[a_A(T - A_s') + b_A\sigma] + 1\} \tag{4}$$

where $0 \leqslant \xi \leqslant 1$ is the Martensite fraction coefficient, ξ_M is the maximum Martensite fraction obtained during cooling, T is the SMA wire temperature, A_s' and A_f' are Austenite phase start and final temperatures, and $a_A = \pi/A_f' - A_s'$, $b_A = -a_A/C_A$ and C_A are curve fitting parameters.

Cooling results in forward transformation from Austenite to Martensite:

$$\xi = \frac{1 - \xi_A}{2}\cos[a_M(T - M_f') + b_M\sigma] + \frac{1 + \xi_A}{2} \tag{5}$$

where ξ_A is the minimum Martensite fraction obtained during heating, M_s' and M_f' are Martensite phase start and final temperatures, and $a_M = \pi/M_s' - M_f'$, $b_M = -a_M/C_M$ and C_M are curve fitting parameters.

The time derivative of Eqs. (4) and (5) yields the state equation during heating:

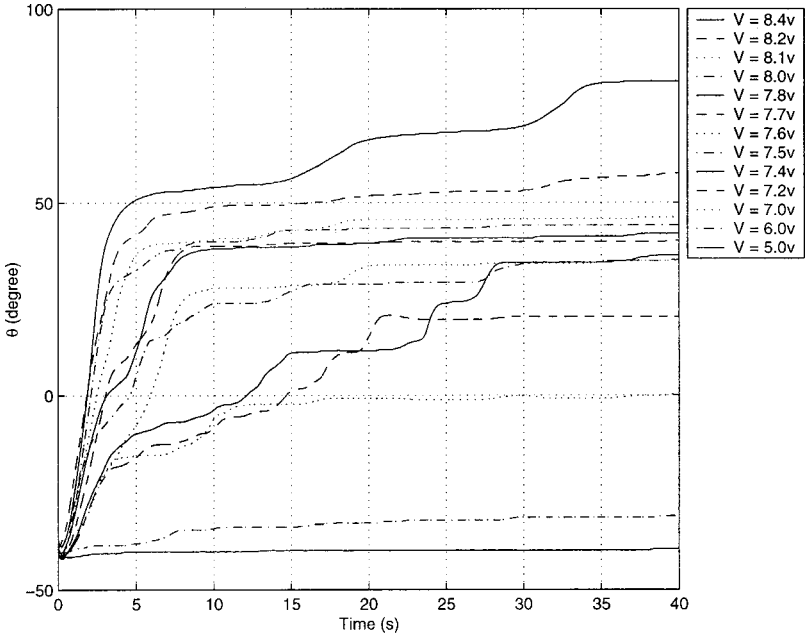

Fig. 4 Open loop experimental results in response to different step inputs

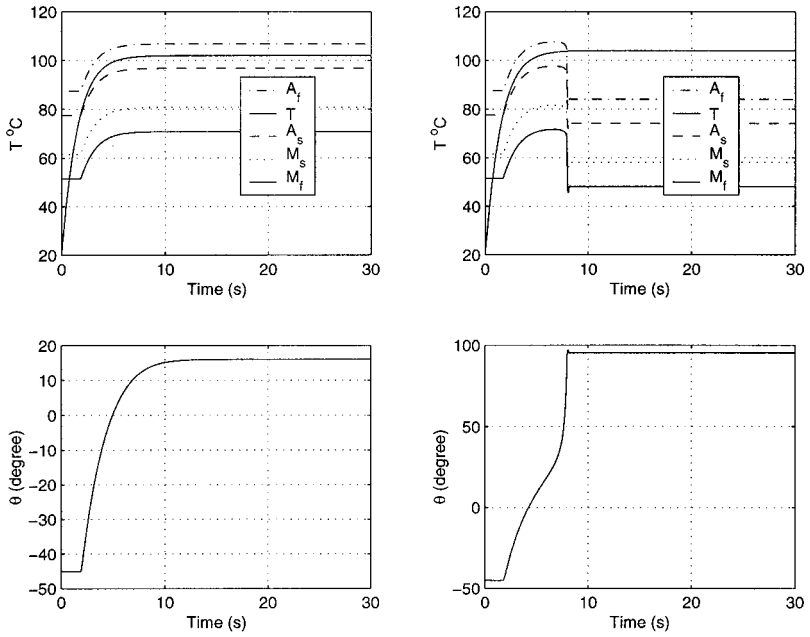

Fig. 5 Effect of a small voltage increase on phase transformation and arm rotation (left) $V=7.2$ v (right) $V=7.3$ v

$$\dot{\xi}=-\frac{\xi_M}{2}\sin[a_A(T-A_s')+b_A\sigma][a_A\dot{T}+b_A\dot{\sigma}] \tag{6}$$

or cooling:

$$\dot{\xi}=-\frac{1-\xi_A}{2}\sin[a_M(T-M_f')+b_M\sigma][a_M\dot{T}+b_M\dot{\sigma}] \tag{7}$$

2.4 Heat Transfer Model. The SMA wire heat transfer equation consists of electrical (joule) heating and natural convection:

$$mc_p\frac{dT}{dt}=\frac{V^2}{R}-hA(T-T_\infty) \tag{8}$$

where V is voltage, R is resistance per unit length, c_p is the specific heat, $m=\rho\pi d^2/4$ is mass per unit length, ρ is density, d is diameter, and $A=\pi d$ is circumferential area of the SMA wire. Also, T_∞ is the ambient temperature and h is heat convection coefficient. We have approximated h by a second order polynomial of temperature to improve the heat transfer model,

$$h=h_0+h_2T^2. \tag{9}$$

2.5 Model Parameters and Simulations. The SMA parameters in this work are predominantly borrowed from Liang [25] and Waram [38]. However, some parameters had to be changed since open loop simulation results did not quantitatively match experimental results (Table 1).

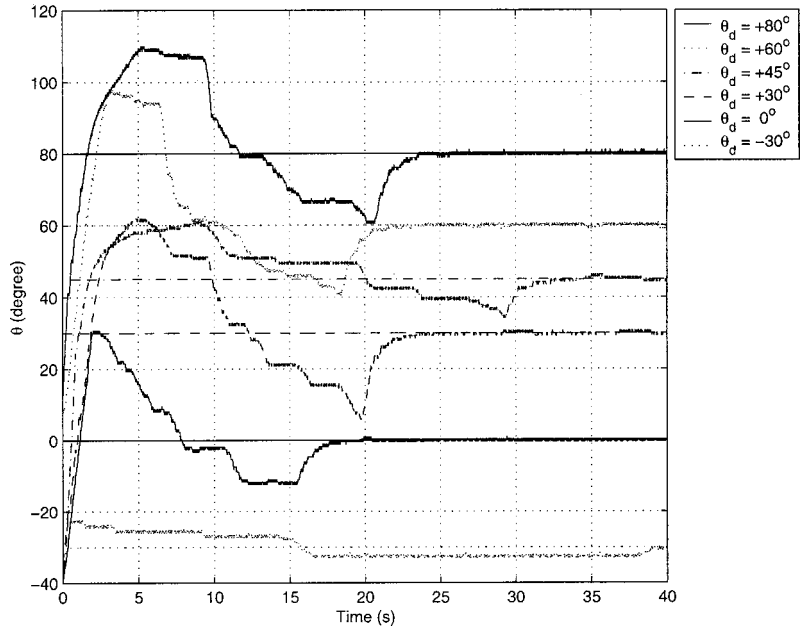

Fig. 6 PID controller experimental results for different desired angles

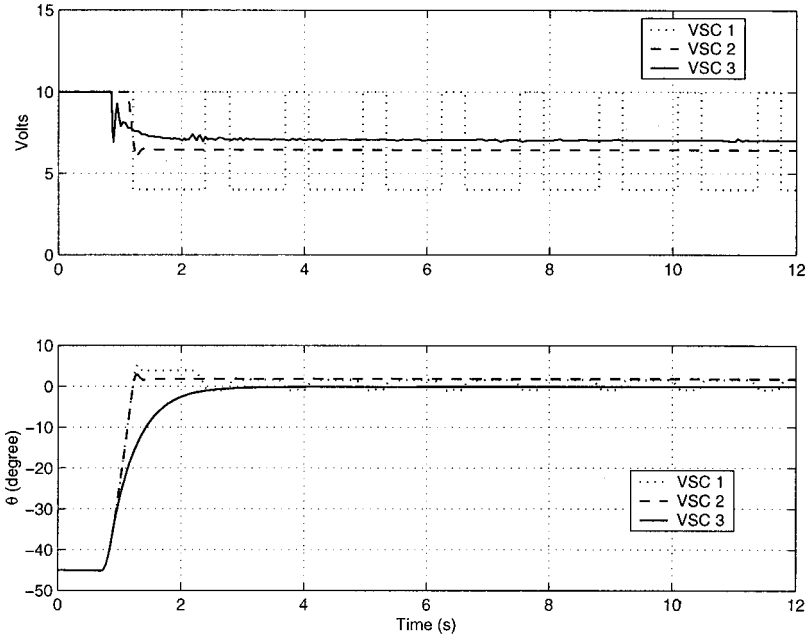

Fig. 7 Simulation results with simple switch (VSC1), simple switch with boundary layer (VSC2), and modified switch with boundary layer (VSC3) controllers; (top) control input *V*, (bottom) system output θ

Although wire resistance is variable, we measured and used an average value. Convection heat transfer polynomial coefficients were measured by matching the simulation and experimental results of the arm angular position. The suggested value for θ_T, by Liang [25], resulted in much larger thermal expansion and contraction effects compared to experimental results. Hence, a significantly lower value was measured and used in this research.

Figures 3 and 4 show the open loop simulation and experimental results in response to incremental step inputs. There are minor differences between simulation and experimental results due to parameter and model uncertainties. However, there is a substantial difference when the input voltage is large enough to cause full actuation due to unmodelled geometry. In these cases, the bias spring touches the stationary link (Fig. 1) and, hence, behaves like a nonlinear hardening spring.

An interesting phenomenon is that at intermediate input voltages, a small increase in the input causes large variations in actuation. This happens because the start and final phases transfor-

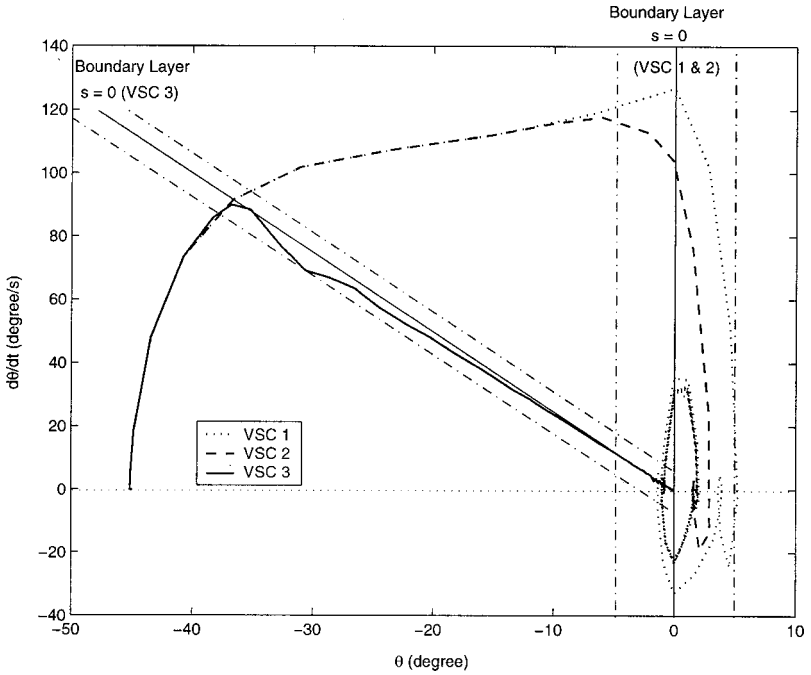

Fig. 8 Phase plane of simulations with simple switch (VSC1), simple switch with boundary layer (VSC2), and modified switch with boundary layer (VSC3) controllers

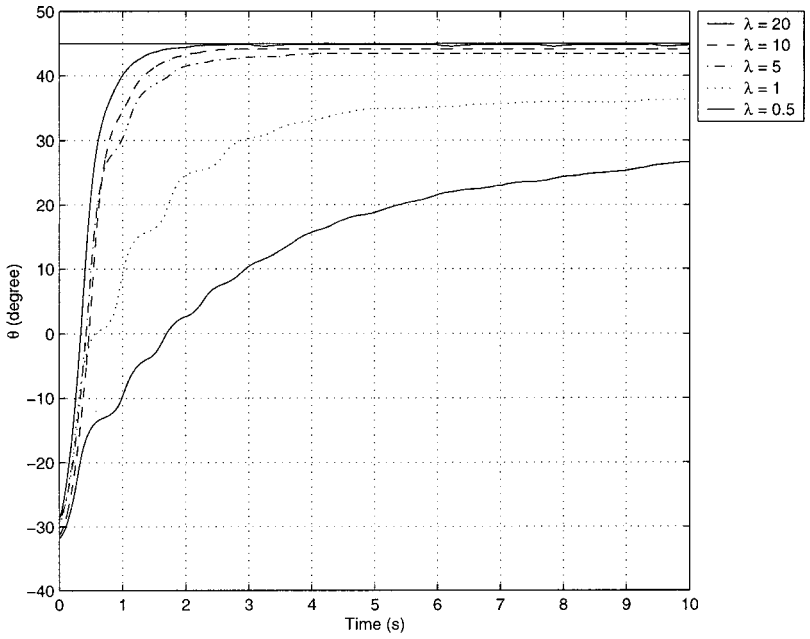

Fig. 9 Modified switch with boundary layer controller experimental results showing the effect of λ

mation temperatures are functions of the SMA wire stress (e.g., $A_s = A_s' + \sigma/C_A$) which reaches its maximum value at an intermediate angle (+30 deg) due to gravity. Figure 5 shows this phenomenon. A small increase ($0.1v$) in the $7.2v$ input results in full transformation (top) and hence full actuation (bottom).

3 Controller Design

The model presented above by Eqs. (1), (8), (3), and (6) (heating) or (7) (cooling) can be represented by a set of nonlinear state equations as

$$\dot{\mathbf{x}} = \mathbf{A}(\mathbf{x},t) + \mathbf{B}(\mathbf{x},\mathbf{u},t) \tag{10}$$

where the state vector $\mathbf{x}$ and the control input $\mathbf{u}$ are given as

$$\mathbf{x} = [\,\theta \;\; \dot{\theta} \;\; T \;\; \sigma \;\; \xi\,] \text{ and } \mathbf{u} = V \tag{11}$$

Note that, some algebraic manipulations are required since Eqs. (3), (6) and (7) are coupled.

The variable structure control is introduced using the switching function $\mathbf{s}(\mathbf{x})$ as [34]:

$$\mathbf{u}(\mathbf{x},t) = \begin{cases} \mathbf{u}^+(\mathbf{x},t) & \text{if } \mathbf{s}(\mathbf{x}) > 0 \\ \mathbf{u}^-(\mathbf{x},t) & \text{if } \mathbf{s}(\mathbf{x}) < 0 \end{cases} \tag{12}$$

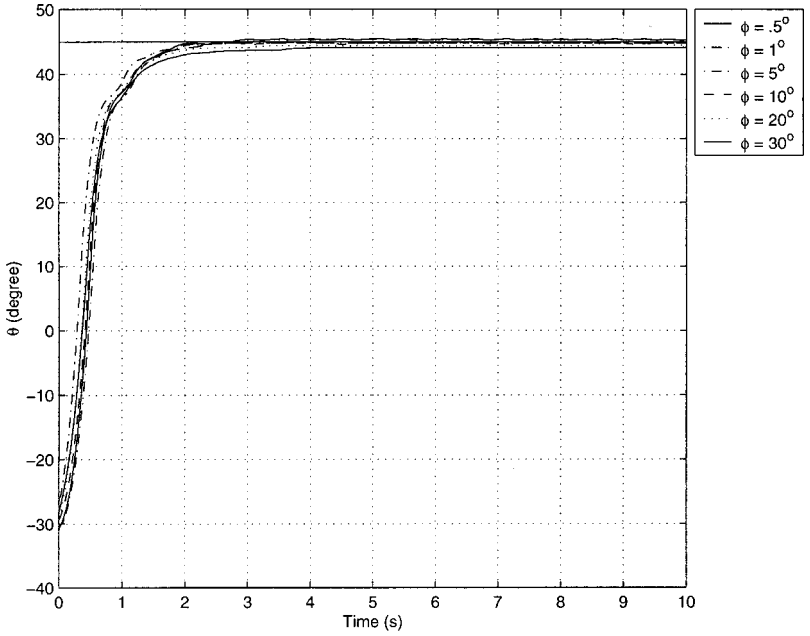

Fig. 10 Modified switch with boundary layer controller experimental results showing the effect of ϕ

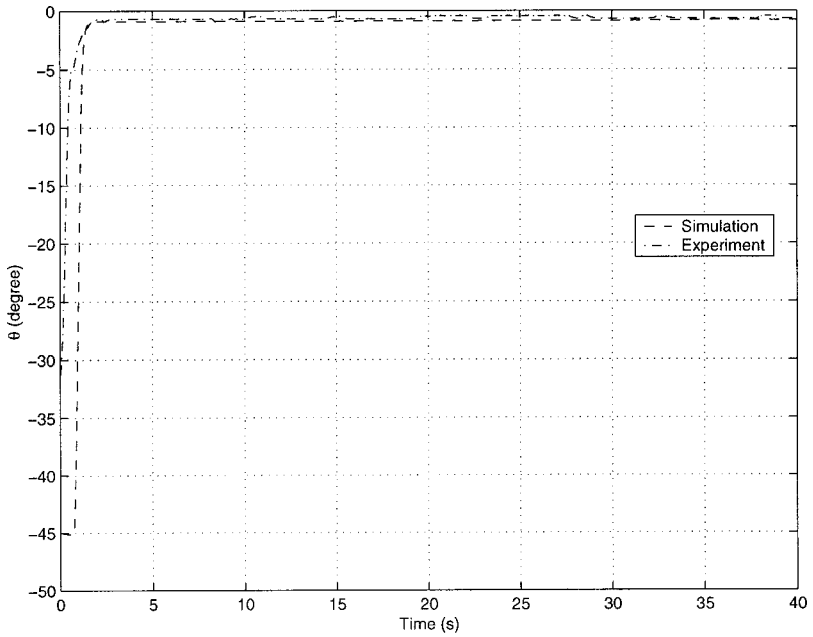

Fig. 11 Comparing simulation and experimental results for modified switch with boundary layer controller (θ_d=0 deg)

such that $\mathbf{s}(\mathbf{x})=0$ (switching surface) can be reached in finite time. The sliding mode takes place on the switching surface, following the desired system dynamics to ensure that the overall VSC system is globally asymptotically stable. Furthermore, a boundary layer around the switching surface can be introduced to avoid chattering which is a common phenomenon in many VSC designs.

3.1 Simple Switch. Initially, we designed a two-stage VSC that is a simple switch between a high voltage for quick heating (i.e., arm rotation) and a low voltage for cooling or reverse motion. The switching is defined based on the position error $s=\tilde{\theta}=\theta-\theta_d$. Hence, system input is defined as

$$\mathbf{u}=\begin{cases} V_{\text{high}} & \text{if } \mathbf{s}<0 \\ V_{\text{low}} & \text{if } \mathbf{s}>0 \end{cases} \tag{13}$$

3.2 Simple Switch With Boundary Layer. Next, a boundary layer is introduced around the switching surface $s=\tilde{\theta}$, to suppress chattering. Denoting the layer thickness as ϕ, the control input is written as

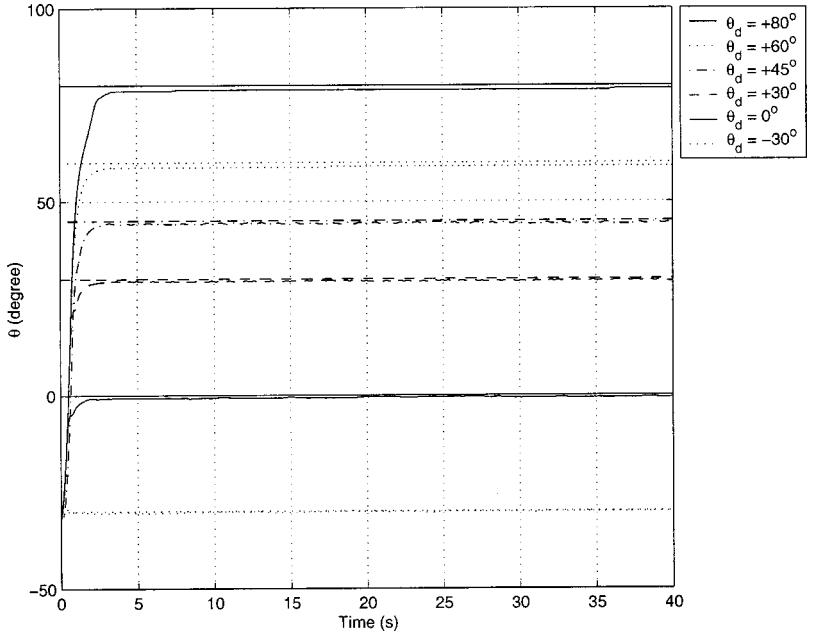

Fig. 12 Modified switch with boundary layer controller experimental results for different desired angles

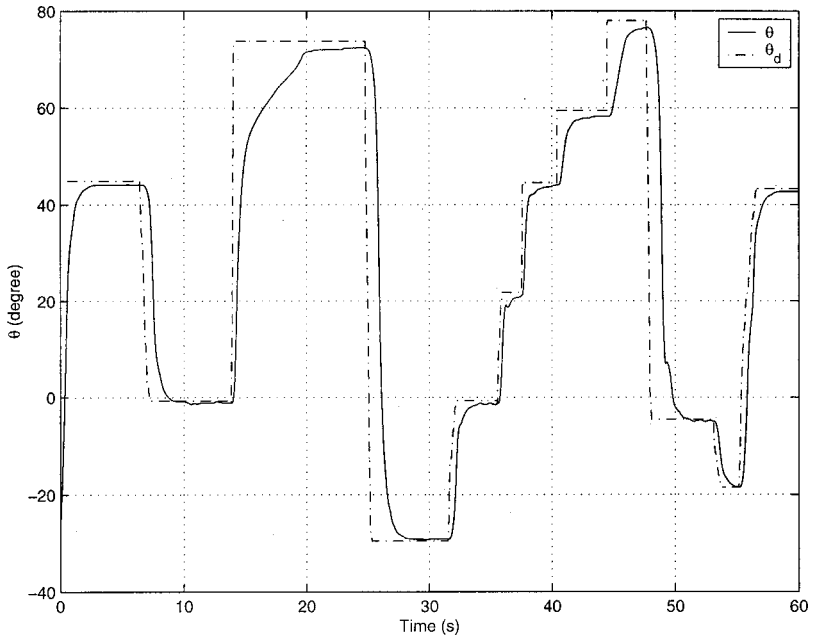

Fig. 13 Modified switch with boundary layer controller experimental results of following user commands

$$\mathbf{u}=\begin{cases} V_{\text{high}} & \text{if} \quad \dfrac{s}{\phi}<-1 \\ V_{\text{low}} & \text{if} \quad \dfrac{s}{\phi}>+1 \\ Ks & \text{if} \quad -1<\dfrac{s}{\phi}<+1 \end{cases} \tag{14}$$

where K is a proportional gain. Generally, increasing the boundary layer thickness, reduces chattering but increases steady-state error.

3.3 Modified Switch With Boundary Layer. The switching condition (surface) introduced above can be modified using a weighted combination of position and velocity errors,

$$s=\left(\frac{d}{dt}+\lambda\right)\tilde{\theta}=\dot{\tilde{\theta}}+\lambda\tilde{\theta} \tag{15}$$

In this system, $-\lambda$ is the slope of sliding surface in the phase plane. Although, the angular velocity is not measured experimentally, a numerical derivative approximation is obtained by filtering out the noise.

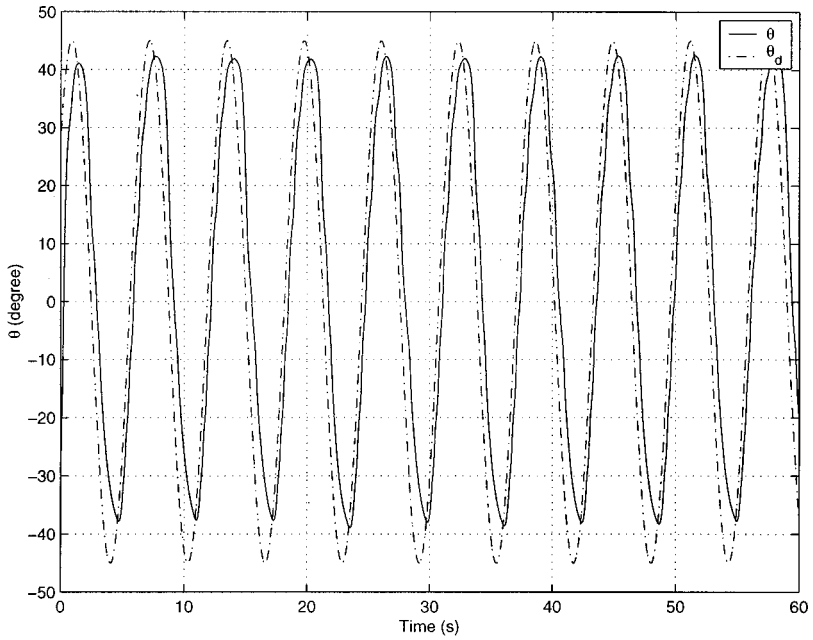

Fig. 14 Modified switch with boundary layer controller experimental results of tracking a sine-wave

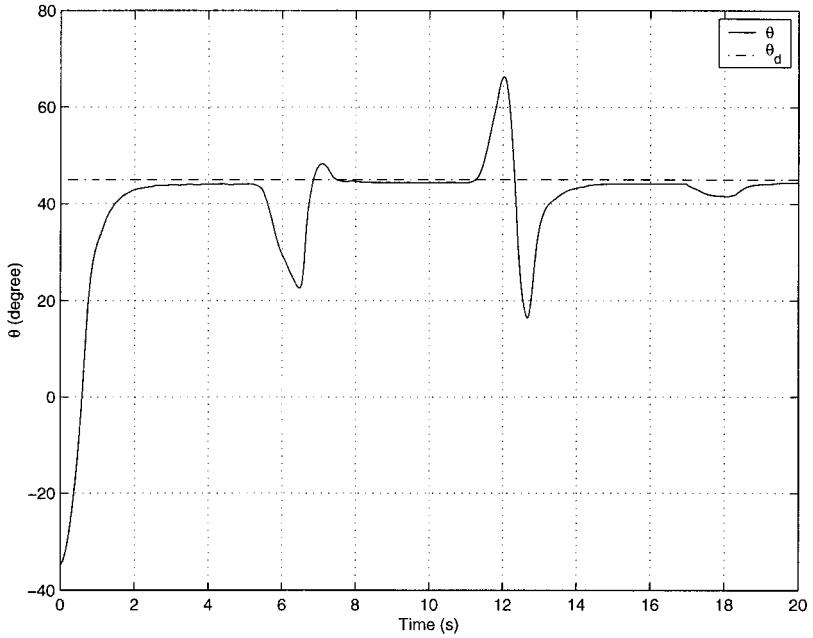

Fig. 15 Modified switch with boundary layer controller experimental results verifying disturbance rejection

4 Results

We started our control experiments by designing a PID controller. Ziegler-Nichols *transient response method* was used to adjust the controller gains K_P, K_I, and K_D. The input to the controller is position error measured by the encoder. System response with PID controller was very slow and inaccurate as shown in Fig. 6.

In the VSC schemes, we chose $V_{\text{high}}=10$ V according to the hardware restrictions and $V_{\text{low}}=4$ V based on simulations and experimental trials. Simulation results for the three controllers are shown in Figs. 7 and 8. The desired position is $\theta_d=0$ deg with zero angular velocity. The simple switch with no boundary layer controller (VSC1) does not achieve a sliding mode and chattering, shown as limit cycle in the phase plane, persists in the response. The addition of boundary layer to the simple switch (VSC2) eliminates chattering. However, there is still an overshoot problem leading to slow settling of the arm (8 sec) due to cooling. Finally, when the simple switch is modified (VSC3), a sliding mode is achieved and the steady state error is greatly reduced. Also, the system response is much faster (3 sec) since there is no overshoot.

The effect of weighting factor on system response is demonstrated experimentally by keeping the boundary layer thickness constant ($\phi=10$ deg), as shown in Fig. 9. Larger λ results in faster system response and smaller steady state error. The limitation is that large λ's could cause overshoot.

The effect of boundary layer thickness, ϕ, is demonstrated experimentally by keeping the weighting factor constant ($\lambda=10$), as shown in Fig. 10. The magnitude of steady state error increases while chattering decreases as ϕ increases, leading to an optimum value between 5 deg to 10 deg for our application. Experimental and simulation results closely agree for modified switch controller with boundary layer as presented in Fig. 11, for one desired angular position ($\theta_d=0°$).

Experimental results verify that the modified switch controller with boundary layer is fast and accurate regardless of the desired angular position, as shown in Fig. 12. The controller is also able to follow commands (Fig. 13) and track different paths such as the sine wave shown in Fig. 14. All three controllers have problems tracking high frequency paths due to physical limitation of the SMA's speed of response.

All three controllers are robust and perform well in the presence of disturbances. Three disturbances are introduced in the form of added payload, reduced payload, and temperature drop. Added and reduced payloads are provided by simple impulsive loads in direction of the gravity and against it, respectively. The temperature drop was imposed by simply blowing air toward the SMA wire. The performance of the modified switch controller in response to these disturbances is shown in Fig. 15.

5 Conclusions

A successful attempt has been made to develop a control algorithm for an SMA-actuated arm. A model for an SMA actuated manipulator has been presented which includes the nonlinear dynamics of the manipulator and constitutive and heat transfer behavior of the SMA wire. Variable Structure Control was used to control this highly nonlinear system. The first design was a simple switch based on position error, which resulted in chattering and overshoot problems. Since the SMA wire cools down through a slow process of natural convection, overshoot (happens because wire is overheated) imposes relatively large delays. In the second design, a boundary layer was added to the control algorithm which eliminated the chattering problem. In the third design, the switch algorithm was modified based on both position and velocity errors. This controller improved performance by eliminating the overshoot problem. The controller was capable of tracking user commands and different paths, along with stabilizing the manipulator at different set points in its workspace. It has been experimentally verified that this controller is fast, robust in the face of parameter uncertainties and unmodelled dynamics, and capable of rejecting disturbances.

Acknowledgments

This paper was compiled under the Concurrent Technologies Corporation's (*CTC*'s) National Applied Software Engineering Center (NASEC) program, which is sponsored by the Defense Advanced Research Projects Agency (DARPA). The content of the information does not necessarily reflect the position or the policy of the government, and no official endorsement should be inferred. The authors would like to acknowledge Dr. S. Santha-

nam and his graduate student S. Bose of the Mechanical Engineering Department at Villanova University for their design of the SMA arm.

References

[1] Biwa, S., Yamada, E., Matsumoto, K., and Shibata, T., 1996, ''Analysis of Bias-Type Actuator Using Shape Memory Alloy Based on Its Thermomechanical Constitutive Description,'' JSME Int. J., Ser. A, **39**(4), pp. 529–532.

[2] Grant, D., and Hayward, V., 1995, ''Design of Shape Memory Alloy Actuator With High Strain and Variable Structure Control,'' *Proceedings of the IEEE International Conference on Robotics and Automation*, pp. 2305–2310.

[3] Hashimoto, M., Takeda, M., Sagawa, H., and Chiba, I., 1985, ''Application of Shape Memory Alloy to Robotic Actuators,'' J. Rob. Syst., **2**(1), pp. 3–25.

[4] Kuribayashi, K., 1986, ''A New Actuator of a Joint Mechanism Using NiTi Alloy Wire,'' Int. J. Robot. Res., **4**(4), pp. 103–108.

[5] Reynaerts, D., and Van Brussel, H., 1991, ''Development of a SMA High Performance Robotic Actuator,'' Fifth International Conference on Advanced Robotics, New York, Vol. 2, pp. 19–27.

[6] Tanaka, Y., and Yamada, A., 1991, ''A Rotary Actuator Using Shape Memory Alloy for a Robot-Analysis of the Response With Load,'' *Proceedings IROS'91, IEEE/RSJ International Workshop on Intelligent Robots and Systems, Intelligence for Mechanical Systems (Cat. No. 91TH0375-6)*, New York, NY, Vol. 2, pp. 1163–1168.

[7] Thomson, P., Balas, G. J., and Leo, P. H., 1995, ''The Use of Shape Memory Alloy for Passive Structural Damping,'' Smart Mater. Struct., **4**(1), pp. 36–41.

[8] Carpenter, B., Head, R. J., and Gehling, R., 1995, ''Shape Memory-Actuated Gimbal,'' Proc. SPIE, **2447**, pp. 91–101.

[9] Gharaybeh, M. A., and Burdea, G. C., 1995, ''Investigation of a Shape Memory Alloy Actuator Force-Feedback Masters,'' Advanced Robotics, **9**(3), pp. 317–329.

[10] Hunter, I., Lafontaine, S., Hollerbach, J., and Hunter, P., 1991, ''Fast Reversible NiTi Fibers for Use in Microrobotics,'' Microelectro-mechanical Systems, Nara, Japan.

[11] Ikuta, K., 1990, ''Micro/Miniature Shape Memory Alloy Actuator,'' IEEE J. Rob. Autom., **3**, pp. 2156–2161.

[12] Liang, C., and Rogers, C. A., 1993, ''Design of Shape Memory Alloy Actuators,'' ASME J. Mech. Des., **114**, pp. 23–30.

[13] Stoeckel, D., and Simpson, J., 1992, ''Actuation and Control With NiTi Shape Memory Alloys,'' *Active Materials and Adaptive Structures, Proceedings of the ADPA/AIAA/ASME/SPIE Conference*, Bristol, UK, IOP Publication, pp. 157–160.

[14] Wen, M., Tu, G. F., Zong, Q. Y., and Xie, C. X., 1994, ''A Study of NiTi Shape Memory Alloy Springs and Its Application in a New Robotic Application,'' *Proceedings of the IEEE International Conference of Industrial Technology (Cat. No. 94TH06593)*, pp. 215–219.

[15] Zerkus, M., and Akers, J., 1992, ''Thermoelectrically Controlled Shape Memory Alloy Actuators,'' *Proceedings of the Conference: Recent Advances in Adaptive and Sensory Materials and their Applications*, Lancaster, PA, Technomic Publishing Co. Inc., pp. 743–754.

[16] Honma, D., Miwa, Y., and Iguchi, N., 1984, ''Micro Robots and Micro Mechanisms Using Shape Memory Alloy,'' *The Third Toyota Conference, Integrated Micro Motion Systems, Micro-machining, Control and Applications*, Nissan, Aichi, Japan.

[17] Kafka, V., 1994, ''A New Concept of Explanation and a Mathematical Modeling, Part I: Micromechanical Explanation of the Causality in the SM Process,'' J. Intell. Mater. Syst. Struct., pp. 809–814.

[18] Arai, S., Aramaki, K., and Yanagisawa, Y., 1994, ''Continuous System Modeling of Shape Memory Alloy (SMA) for Control Analysis,'' *Proceedings of the 5th IEEE International Symposium on Micro Machine and Human Science*, pp. 97–99.

[19] Ikuta, K., Tsukamoto, M., and Hirsoe, S., 1991, ''Mathematical Model and Experimental Verification of Shape Memory Alloy for Designing Micro Actuator,'' *Proceedings of the IEEE MicroElectroMechanical Systems Conference*, pp. 103–108.

[20] Madill, D., and Wang, D. R., 1998, ''Modeling and L2-Stability of a Shape Memory Alloy Position,'' IEEE Trans. Control Syst. Technol., **6**(4), pp. 473–481.

[21] Tanaka, Y., and Nagaki, S., 1982, ''A Thermomechanical Description of Materials With Internal Variables in the Process of Phase Transformation,'' Ingenieur-Archive, **51**, pp. 287–299.

[22] Tanaka, Y., and Iwasaki, A., 1985, ''A Phenomenological Theory of Transformation Superplasticity,'' Eng. Fract. Mech., **21**(4), pp. 709–720.

[23] Tanaka, Y., 1986, ''A Thermomechanical Sketch of Shape Memory Effect: One-Dimensional Tensile Behavior,'' Res. Mech., **18**(1), pp. 251–263.

[24] Webb, D. C., Lagoudas, G. V., and Kurdila, A. J., 1998, ''Hysteresis modeling of SMA Actuators for Control Applications,'' J. Intell. Mater. Syst. Struct., **9**(6), pp. 432–448.

[25] Liang, C., and Rogers, C. A., 1990, ''One-Dimensional Thermomechanical Constitutive Relations for Shape Memory Materials,'' J. Intell. Mater. Syst. Struct., **1**(2), pp. 207–234.

[26] Shahin, Ali R., Meckl, Peter H., Jones, James D., and Thrasher, Mark A., 1994, ''Enhanced Cooling of Shape Memory Alloy Wires Using Semiconductor Heat Pump Modules,'' J. Intell. Mater. Syst. Struct., **5**(1), pp. 95–104.

[27] Gorbet, R. B., and Wang, D. W. L., 1995, ''General Stability Criteria for a Shape Memory Position Control Systems,'' *Proceedings of IEEE International Conference on Robotics and Automation*, **3**, pp. 2313–2319.

[28] van der Wijst, M. W. M., Schreurs, P. J. G., and Veldpaus, F. E., 1997, ''Application of Computed Phase Transformation Power to Control Shape Memory Alloy Actuators,'' Smart Mater. Struct., **6**(2), pp. 190–198.

[29] Nakazato, T., Kato, Y., and Masuda, T., 1993, ''Control of Push-Pull-Type Shape Memory Alloy Actuators by Fuzzy Reasoning,'' Trans. Jpn. Soc. Mech. Eng., Ser. C, **59**(568), pp. 226–232.

[30] Kumagai, P., Hozian, A., and Kirkland, M., 2000, ''Neuro-Fuzzy Model Based Feed-Back Controller for Shape Memory Alloy Actuators,'' Proc. SPIE, **3984**, pp. 291–299.

[31] Dickinson, C. A., and Wen, J. T., 1998, ''Feedback Control Using Shape Memory Alloy Actuators,'' J. Intell. Mater. Syst. Struct., **9**(4), pp. 242–250.

[32] Arai, S., Aramaki, K., and Yanagisawa, Y., 1995, ''Feedback Linearization of SMA (Shape Memory Alloy),'' *Proceedings of the 34th SICE Annual Conference*, pp. 519–522.

[33] Choi, S., and Cheong, C. C., 1996, ''Vibration Control of Flexible Beam Using Shape Memory Alloy Actuators,'' J. Guid. Control Dyn., **19**(5), pp. 1178–1180.

[34] Stepanenko, Y., and Su, C. Y., 1992, ''Variable Structure Control of Robot Manipulators With Nonlinear Sliding Manifolds,'' Int. J. Control, **58**(2), pp. 285–300.

[35] Grant, D., and Hayward, V., 1997, ''Variable Structure Control of Shape Memory Alloy Actuators,'' IEEE Systems and Control Magazine, **17**(3), pp. 80–88.

[36] Grant, D., and Hayward, V., 1998, ''Vibration Isolation with High Strain Shape Memory Alloy Actuators: Case of the Impulse Disturbance,'' *Proceedings of International Mechanical Engineering Congress and Exposition*, p. 229.

[37] Grant, D., and Hayward, V., 2000, ''Constrained Force Control of Shape Memory Alloy Actuators,'' *Proceedings of the IEEE International Conference on Robotics and Automation*, pp. 1314–1320.

[38] Waram, T., *Actuator Design Using Shape Memory Alloys*, T. C. Waram., Ontario L8S 1L8, Canada, second edition, 1993.